Experimental Observation of *PT* Symmetry Breaking near Divergent Exceptional Points

M. Sakhdari,[1] M. Hajizadegan,[1] Q. Zhong,[2] D. N. Christodoulides,[3] R. El-Ganainy,[2,*] and P.-Y. Chen[1,†]
[1]*Department of Electrical and Computer Engineering, University of Illinois at Chicago, Chicago, Illinois 60607, USA*
[2]*Department of Physics and Henes Center for Quantum Phenomena, Michigan Technological University, Houghton, Michigan, 49931, USA*
[3]*College of Optics & Photonics-CREOL, University of Central Florida, Orlando, Florida 32816, USA*

(Received 8 July 2019; revised manuscript received 5 September 2019; published 7 November 2019)

Standard exceptional points (EPs) are non-Hermitian degeneracies that occur in open systems. At an EP, the Taylor series expansion becomes singular and fails to converge—a feature that was exploited for several applications. Here, we theoretically introduce and experimentally demonstrate a new class of parity-time symmetric systems [implemented using radio frequency (rf) circuits] that combine EPs with another type of mathematical singularity associated with the poles of complex functions. These nearly divergent exceptional points can exhibit an unprecedentedly large eigenvalue bifurcation beyond those obtained by standard EPs. Our results pave the way for building a new generation of telemetering and sensing devices with superior performance.

DOI: 10.1103/PhysRevLett.123.193901

Spectral points that possess special features have been a subject of intense study recently. A well-known example of such points that are pertinent to periodic systems is the van Hove singularity, at which the optical density of state does not vary smoothly as a function of frequency. First investigated in the context of lattice vibrations [1], and later in photonic crystals [2], identifying these points has been proven useful in spectroscopy applications [3]. Another important class of spectral points are those associated with the eigenvalue degeneracy of Hermitian Hamiltonians [widely known as diabolic points (DPs)], which play an important role in the studies of molecular vibrations within the so called Born-Oppenheimer approximation. In the theory of band structures, a DP associated with a dispersionless band is also known as a Dirac point [4,5] (since it also arises from the relativistic Dirac equation). While Dirac points are not associated with any topological protection, a close cousin, known as a Weyl point, further offers topological features [6–8]. Despite the fact that these mathematical constructions have been known for several decades, it was not until recently that physicists were able to experimentally probe them in the laboratory, especially in optical platforms where many-body interactions can be controlled at will.

The aforementioned work focused mainly on Hermitian systems. Relaxing this condition to deal with effective non-Hermitian systems can result in even more exotic spectral features. More specifically, the non-Hermiticity of an effective Hamiltonian implies that its eigenstates do not need to be orthogonal. As a result, special degeneracies where both the eigenvalues and eigenfunctions become the same can occur at the so called exceptional points (EPs) [9–14]. The interest in the peculiar behavior associated with EPs has exploded in the past years following the discovery of parity-time (*PT*) symmetric Hamiltonians that exhibit real spectra [15], and the introduction of this concept to classical wave dynamics for the first time [16–19], which opened the door for a host of experimental studies in optics [20–22] and electronics [23–31] as well as other platforms. Currently, several research groups are exploring the utility of non-Hermitian optics near EP to build miniaturized optical isolators [32,33], better lasers [20–22,34–41], more responsive sensors [42–47], and nonlinear optical devices [48,49] to mention just a few examples. For recent reviews, see [50,51]. Additionally, enhanced wireless sensing with EPs has also attracted attention recently [25–31].

Despite this progress, all these activities focused only on one type of EP having the form $\sqrt[n]{\cdot}$. These represent branch point singularities at which the tailor series expansion of the associated function fails to exist. However, apart from the discontinuity across the branch cut (with its intriguing implications for the encircling of EPs [52–54]), the eigenvalues themselves (or equivalently, the associated multivalued function) remain bounded.

In this Letter, we consider a rather unusual scenario where an EP coincides with (or occurs in the vicinity of) a divergent singularity. We show that, even though in practice physical systems cannot diverge, they can be locked near a divergent EP (DEP). Particularly, we show theoretically and demonstrate experimentally that the effect of a DEP on a nearby nondivergent EP can leave a clear fingerprint featured by giant enhancement of the eigenvalue splitting across the latter.

To this end, and before we describe our experimental results, let us consider a function of the form $f(x) = (1/\sqrt{1-x^2})$. The function f is real valued for $x < 1$ and

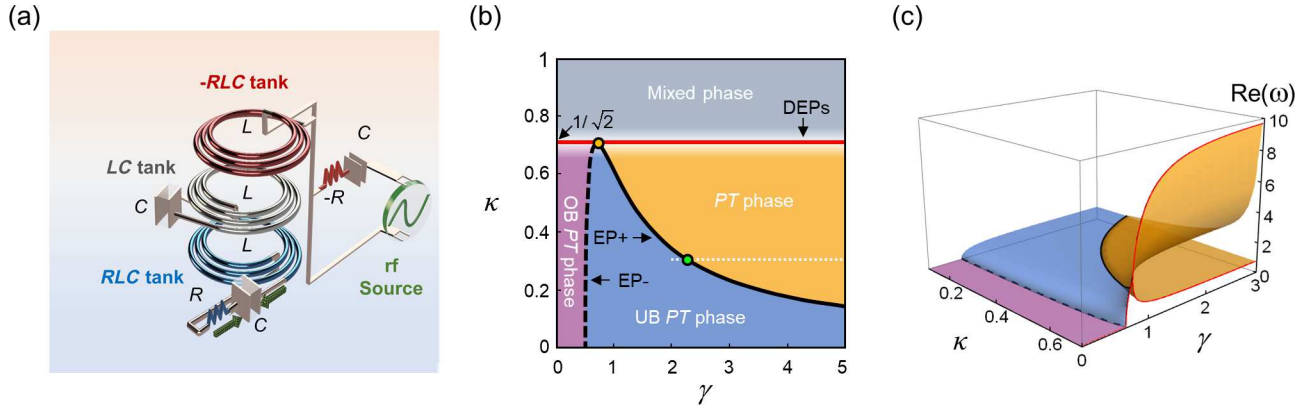

FIG. 1. (a) A schematic of the three-element PT-symmetric electronic circuit proposed for implementing nearly divergent EPs. It consists of a $-RLC$ gain tank (top red), an RLC loss tank (bottom blue) and a neutral element LC (center gray). The normalized coupling between the coils is κ and the non-Hermitian parameter is γ (see text for definition). (b) The phase diagram of this circuit in the κ–γ plane. As discussed in the text, four different phases are identified: PT symmetry, underdamped broken PT symmetry (UB PT), overdamped broken PT symmetry (OB PT) and a mixed phase that contains eigenstates in the PT phase and others in the broken phase. The black solid and dashed lines, denoted by EP±, are exceptional lines that separate different phases. The solid red line consists of divergent EPs and separates the mixed phase from the rest of the domains. The white dashed line indicates the parameters used for the experiment as discussed later. (c) Bifurcation of real parts of the eigenvalues associated with (b). Note that as $\kappa \to \kappa_D = 1/\sqrt{2}$, the splitting between the eigenfrequency becomes larger (theoretically diverges when $\kappa = \kappa_D$).

imaginary for $x > 1$ with an EP located at $x = 1$, which is also the same point where the function diverges, i.e., $f(1) = \infty$. As a result, in contrast to standard EPs where the splitting of the real part scales smoothly (for example, as a square root function for second-order EPs), here, it diverges abruptly. If one could implement this system experimentally, it would be the ultimate sensor with infinite responsivity to any infinitesimal perturbation. Unfortunately, in practice, this is not possible. Many realistic physical effects (such as the existence of a source at very high frequencies, stabilities, and nonlinearities) will come into play to prevent such a response. Thus, it may seem that this concept is of little practical use. However, before we give up, let us consider a related function that has an additional degree of freedom: $F(x, y) = \sqrt{\alpha_1^2 - y^2}/\sqrt{\alpha_2^2 - x^2}$. Assuming $\alpha_1 \neq \alpha_2$, the function $F(x, y)$ will have a standard exceptional line at $y = \alpha_1$ and a divergent singularity at $x = \alpha_2$. If one can design a system that operates close enough to $x = \alpha_2$, the divergent point will be avoided, while at the same time its impact will be imprinted on the eigenvalue splitting across the exceptional line $y = \alpha_1$: the closer we get to $x = \alpha_2$, the larger the eigenvalue bifurcation. In this case, we call the EP $y = \alpha_1$ nearly divergent or NDEP (in the above example, it is actually a line rather than a point, but this is irrelevant to the subsequent discussion).

Having introduced the notion of DEPs and NDEPs theoretically, it is natural to inquire about the possibility of building a physical system that exhibits these spectral features. Indeed, this is a challenging task given that optical systems (the most widely used platform for investigating non-Hermitian physics) do not naturally exhibit these spectral divergences, due to a lack of lumped elements (in which the current does not vary, i.e., phase change or transition time is negligible). In this regard, radio frequency (rf) quasistatic resonators made of RLC circuits [consisting of a resistor (R), an inductor (L), and a capacitor (C)] provide an advantage: in coupled PT electronic systems (composed of two coupled $-RLC$ and RLC resonators), the solution of the second-order differential equations arising from Kirchhoff current and voltage laws exhibit such a singularity [23,26]. However, it occurs only for a perfect mutual coupling between the inductors, a condition that is impossible to achieve in practice. To complicate things further, it is not even easy to design a system that operates near this point. In practice, a nearly perfect inductive coupling requires a high permeability magnetic core and shielding plates, and any material or Eddy-current loss could decrease the coupling coefficient significantly [55].

In order to proceed, let us consider a coupled electronic circuit that consists of three stages representing gain, neutral, or loss resonators, as shown in Fig. 1(a). We will denote this circuit with C_3 (as opposed to the standard two-element PT circuit which we will denote C_2). One may think that adding a neutral element may lead to a standard higher order EP similar to the counterpart optical systems [56–58]. However, this is not the case. By applying Kirchhoff laws to the proposed circuit topology shown in Fig. 1(a). we can write an effective PT-symmetric Hamiltonian for the system, H_{eff}, with the following eigenfrequencies [see the Supplemental Material (SM) [59] for more details]

$$\omega_n = \pm 1, \pm\sqrt{\frac{2\gamma^2 - 1 \pm \sqrt{1 - 4\gamma^2 + 8\gamma^4\kappa^2}}{2\gamma^2(1 - 2\kappa^2)}}, \qquad (1)$$

where $\gamma = R^{-1}\sqrt{L/C}$ is the non-Hermitian parameter and $\kappa = M/L < 1$ is the normalized mutual coupling (here, M and L are mutual and self inductances of the coils). By inspecting Eq. (1), it is clear that $\kappa = \kappa_D \equiv 1/\sqrt{2}$ are the DEPs. For $\kappa < \kappa_D$, we can identify three different phases, separated by two exceptional lines described by the equations $\gamma_{EP\pm} = \sqrt{1 \pm \sqrt{1-2\kappa^2}}/(2\kappa)$, as shown as black solid or dashed lines in Fig. 1(b). In the PT phase given by $\gamma \in [\gamma_{EP+}, +\infty]$, all the eigenstates respect PT symmetry with real eigenvalues. In the range $\gamma \in [\gamma_{EP-}, \gamma_{EP+}]$, the system exhibits an underdamped broken PT (UB PT) phase where the eigenvalues are complex conjugate. In the overdamped broken PT (OB PT) phase with $\gamma \in [0, \gamma_{EP-}]$, the eigenvalues are purely imaginary. Mathematically, the last two regimes are separated by an exceptional line. This feature arises due to charge conjugation symmetry of the Hamiltonian: $H = -H^*$ (see the SM [59] for details). However, we note that, physically, the solutions related by this symmetry correspond to the same state. For $\kappa > \kappa_D$, the eigenspectrum exhibits a mix between PT states and broken PT states. The boundary separating this mixed phase from the rest of the phase diagram is marked by a divergent exceptional line: a line made of DEPs, i.e., EPs that also coincide with pole singularities. Note that the three exceptional lines (black solid, black dashed, and red lines) meet at one point given by $(\gamma, \kappa) = (1/\sqrt{2}, 1/\sqrt{2})$. It is important to emphasize that, before the system approaches this divergent regime, nonlinear effects dominated by the nonlinearity of the active circuit element (which is used to implement the negative resistance as discussed in the SM [59]) will come into play to regulate the circuit behavior. Thus, the important question is, can one at least engineer the system to operate close enough to these DEPs such that they have significant impact on the spectral features? Figure 1(c) plots the linear spectrum associated with Eq. (1). It shows that close to the DEPs, the eigenvalue's bifurcation (which corresponds to frequency splitting between two resonant frequencies, not to their amplitudes) becomes dramatic—a feature that can be utilized to build next generation ultra-responsive PT sensors beyond the current state of the art. In theory, similar behavior can also be traced in the conventional two-element PT symmetric systems studied in [23]. In practice, the divergent exceptional line in the latter occurs for $\kappa = 1$—a condition that is impossible to achieve in experiment as it implies perfect mutual coupling between the inductors, i.e., equal values for the mutual and self inductances. Thus, the main merit of the three-element circuit presented here is to bring these singularities to an experimentally accessible domain. Importantly, we note that the above results do not have analogs in optical systems. In fact, an optical PT trimer that consists of a neutral element sandwiched between gain and loss sites will demonstrate a very different behavior by possessing a third order exceptional point [45,56–58].

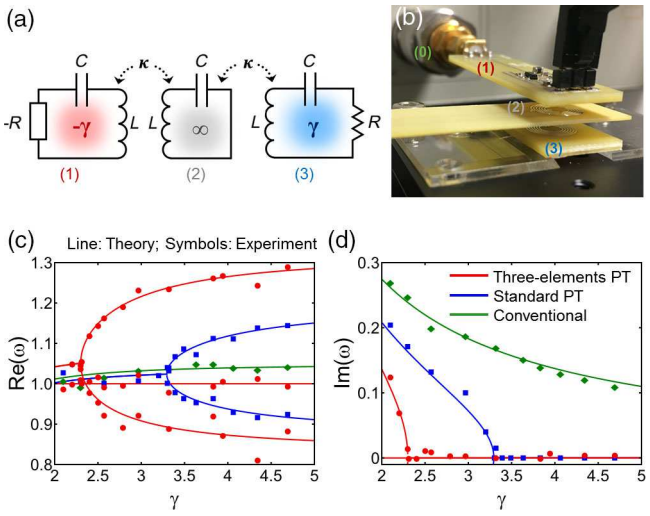

FIG. 2. Circuit schematic (a) and picture of the on-board circuit implementation (b) of the proposed three-elements rf network. (c) and (d) plot the real and imaginary eigenfrequencies as extracted from the rf reflection measurements (see the SM [59] for details). From (c), it is clear that the frequency splitting in the proposed system (red lines and dots) is larger than that of the corresponding standard PT system having a coupling $\kappa = 0.3$ (blue lines and dots), as well as that associated with a conventional telemetry system based on non-PT inductive coupling geometry (see Fig. S.2 in the SM [59] for more details) which is shown in green lines and dots [26].

In order to demonstrate the advantage of the proposed circuit topology [Fig. 1(a)] in providing indirect access to the DEPs with potential telemetric sensing applications, we have built a prototype using onboard circuit technology (see the SM [59] for details). The circuit consists of a tunable RLC tank that mimics a wireless capacitive sensor [26]. This pseudosensor consists of a variable capacitor, connected in series to a planar spiral inductor and a resistor (which accounts for the effective resistance of the sensor), such that its equivalent circuit is identical to that of a realistic wireless sensor. The information provided by the sensor is then read by a $-RLC$ tank connected to the vector network analyzer for measuring the reflection spectrum. Unlike standard PT-symmetric telemetric systems where the sensor and reader tanks are directly coupled [26], the current system is constructed by inserting a neutral LC tank between the $-RLC$ and RLC oscillators as shown in Fig. 1(a). In both the $-RLC$ and RLC resonators, the inductance of microstrip coils is $L = 330\text{nH}$ and the absolute value of resistance $|-R| = R = 50\ \Omega$. In order to emulate behaviors of a wireless capacitive sensor, the capacitance C of tank circuits is tuned from 30 to 220 pF (SMA CER $\pm$ 0.05 pF). This, in turn, varies the non-Hermitian parameter of the system, $\gamma \propto 1/\sqrt{C}$ which is the relevant parameter for real-life wireless capacitive sensing applications [26]. A schematic diagram and a picture of the implemented circuit are shown in Figs. 2(a) and 2(b), respectively. For comparison, we have

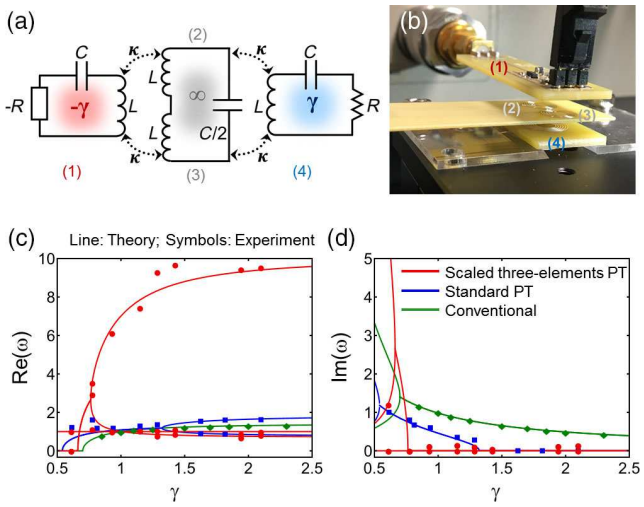

FIG. 3. Schematic of the scaled three-element circuit (a) and picture of its on-board circuit implementation (b). (c), and (d) plot the real and imaginary eigenfrequencies, varying a function of non-Hermitian parameter γ, for the dual-links three-stages PT-symmetric telemetric system in (a) with $\kappa = 0.495$ (red circles), the standard PT-symmetric telemetric system with $\kappa = 0.7$ (blue squares), and the conventional one using a microcoil reader with $\kappa = 0.7$ (green diamonds). A fivefold enhancement in the bifurcation compared to a standard PT circuit is observed. For comparison, we also present the results for conventional a telemetry system (green line and dots) [26]. For completeness, we also plot the constant eigenfrequency (horizontal red line) associated with the solution in Eq. (1).

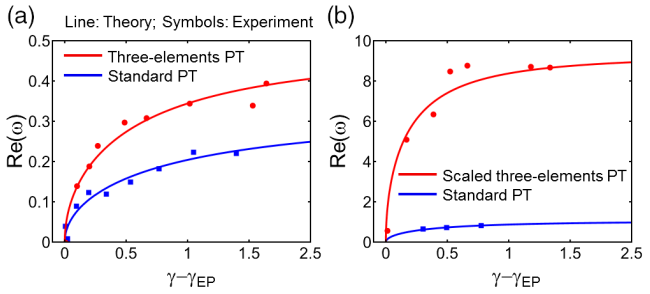

FIG. 4. Plots of the frequency splitting as a function of $\Delta\gamma = \gamma - \gamma_{EP}$ for both experimental setups shown in Figs. 2 and 3. Note that the scaled PT circuit offers a clear advantage as measured by larger splitting.

also fabricated a standard (two-element) PT circuit. In both structures, the normalized coupling coefficient was engineered to be $\kappa = 0.3$. While this value is relatively weak, it still favors the three-element circuit in terms of operation near the DEP (corresponding to $\kappa \approx 0.7$) as compared to the standard two-element circuit having DEP at $\kappa = 1$.

Figures 2(c) and 2(d) plot the theoretical (solid lines) and experimental (dots) values of complex eigenfrequencies as a function of the non-Hermitian parameter γ for the proposed three-element circuit. The experimental results here span the range indicated by the white dashed line in Fig. 1(b); i.e., they trace the transition from the UB PT phase to the PT phase across the EP marked by the green point in the figure. For comparison, we also present the results for the standard two-element PT circuit on the same figure. First, we find a good agreement between theoretical predictions and experimental data. Second, it is clear that the three-element system demonstrates giant frequency splitting (red data points) compared with the standard one (blue dots). Finally, we also note that the location of the EP in the proposed three-element system is down shifted compared with the standard circuit, which is in agreement with theory.

Encouraged by these results, we have also explored the related system shown in Fig. 3(a). Here, the neutral oscillator has the same resonant frequency as before but with its inductor and capacitor scaled according to $2L$ and a $C/2$. Furthermore, we consider the coupling topology shown in Fig. 3(a). By following a similar analysis to that shown in the SM [59], one can show that the new frequency splitting will be enhanced because κ in Eq. (1) is replaced by $\sqrt{2}\kappa$. In this case, the divergent exceptional line is located at $\kappa_D = 0.5$. In other words, this modified circuit requires reduced normalized coupling to bring the system closer to the DEP, which in turn, leads to enhanced eigenvalue bifurcation. Figure 3(b) depicts the fabricated circuit with the modified neutral circuit. The theoretical and experimental data for the spectral bifurcation are plotted in Figs. 3(c) and 3(d). Again for comparison, we also plot the data for the standard two-element PT circuit. As evidenced by the plots, we observe a gigantic enhancement of the frequency bifurcations, almost 5 times more than in the previous case.

To further facilitate the comparison between the proposed circuits with respect to each other as well as to the standard PT circuit, we also plot the frequency splitting extracted from Figs. 2 and 3 as a function of $\Delta\gamma = \gamma - \gamma_{EP}$. As can be observed from Figs. 4(a) and 4(b), the scaled PT circuit, being closer to the DEP, offers a clear advantage as measured by larger splitting.

In conclusion, we have introduced the notion of divergent exceptional points and showed how they can be indirectly accessed by using three-element PT-symmetric electronic circuits made of gain-neutral-loss resonators. We have tested our predictions experimentally and demonstrated that, indeed, the eigenfrequency bifurcation close to divergent exceptional points can be boosted as a result of the interplay between the square root splitting of second order EPs and the giant multiplication factor associated with DEPs. We envision that such new non-Hermitian electronic systems, when applied to wireless probing and telemetering, will enable a superior sensing capability. This work can also be extended to other microwave, millimeter-wave and terahertz wireless systems.

R. E. is supported by the Army Research Office (ARO) Grant No. W911NF-17-1-0481, and the National Science Foundation (NSF) Grant No. ECCS 1807552. P.-Y. C. is

supported by NSF Grant No. ECCS 1914420: CAREER, and UIC DPI Cycle 2 Seed Funding Program.

M. S., M. H. and Q. Z. contributed equally to this manuscript.

*Corresponding author.
ganainy@mtu.edu
†Corresponding author.
pychen@uic.edu

[1] L. van Hove, Phys. Rev. **89**, 1189 (1953).
[2] M. Ibanescu, E. J. Reed, and J. D. Joannopoulos, Phys. Rev. Lett. **96**, 033904 (2006).
[3] M. S. Dresselhaus, G. Dresselhaus, A. Jorio, A. G. Souza Filho, and R. Saito, Carbon **40**, 2043 (2002).
[4] X. Huang, Y. Lai, Z. H. Hang, H. Zheng, and C. T. Chan, Nat. Mater. **10**, 582 (2011).
[5] R. A. Sepkhanov, Y. B. Bazaliy, and C. W. J. Beenakker, Phys. Rev. A **75**, 063813 (2007).
[6] L. Lu, L. Fu, J. D. Joannopoulos, and M. Soljačić, Nat. Photonics **7**, 294 (2013).
[7] L. Lu, J. D. Joannopoulos, and M. Soljačić, Nat. Photonics **8**, 821 (2014).
[8] L. Lu, Z. Wang, D. Ye, L. Ran, L. Fu, J. D. Joannopoulos, and M. Soljačić, Science **349**, 622 (2015).
[9] W. D. Heiss and A. L. Sannino, J. Phys. A **23**, 1167 (1990).
[10] A. I. Magunov, I. Rotter, and S. I. Strakhova, J. Phys. B **32**, 1669 (1999).
[11] W. D. Heiss, J. Phys. A **37**, 2455 (2004).
[12] W. D. Heiss, J. Phys. A **45**, 444016 (2012).
[13] I. Rotter, Phys. Rev. E **67**, 026204 (2003).
[14] M. Müller and I. Rotter, J. Phys. A **41**, 244018 (2008).
[15] C. M. Bender and S. Boettcher, Phys. Rev. Lett. **80**, 5243 (1998).
[16] C. E. Rüter, K. G. Makris, R. El-Ganainy, D. N. Christodoulides, M. Segev, and D. Kip, Nat. Phys. **6**, 192 (2010).
[17] K. G. Makris, R. El-Ganainy, D. N. Christodoulides, and Z. H. Musslimani, Phys. Rev. Lett. **100**, 103904 (2008).
[18] Z. H. Musslimani, K. G. Makris, R. El-Ganainy, and D. N. Christodoulides, Phys. Rev. Lett. **100**, 030402 (2008).
[19] R. El-Ganainy, K. G. Makris, D. N. Christodoulides, and Z. H. Musslimani, Opt. Lett. **32**, 2632 (2007).
[20] B. Peng, Ş. K. Özdemir, S. Rotter, H. Yilmaz, M. Liertzer, F. Monifi, C. M. Bender, F. Nori, and L. Yang, Science **346**, 328 (2014).
[21] L. Feng, Z. J. Wong, R.-M. Ma, Y. Wang, and X. Zhang, Science **346**, 972 (2014).
[22] H. Hodaei, M.-A. Miri, M. Heinrich, D. N. Christodoulides, and M. Khajavikhan, Science **346**, 975 (2014).
[23] J. Schindler, A. Li, M. C. Zheng, F. M. Ellis, and T. Kottos, Phys. Rev. A **84**, 040101(R) (2011).
[24] M. Chitsazi, H. Li, F. M. Ellis, and T. Kottos, Phys. Rev. Lett. **119**, 093901 (2017).
[25] S. Assawaworrarit, X. Yu, and S. Fan, Nature (London) **546**, 387 (2017).
[26] P.-Y. Chen, M. Sakhdari, M. Hajizadegan, Q. Cui, M. M.-C. Cheng, R. El-Ganainy, and A. Alú, Nat. Electron. **1**, 297 (2018).
[27] M. Sakhdari, M. Hajizadegan, Y. Li, M. M. Cheng, J. C. H. Hung, and P.-Y. Chen, IEEE Sens. J. **18**, 9548 (2018).
[28] M. Hajizadegan, M. Sakhdari, S. Liao, and P.-Y. Chen, IEEE Trans. Antennas Propag. **67**, 3445 (2019).
[29] P.-Y. Chen and J. Jung, Phys. Rev. Applied **5**, 064018 (2016).
[30] Z. Dong, Z. Li, F. Yang, C.-W. Qiu, and J. S. Ho, Nat. Electron. **2**, 335 (2019).
[31] P.-Y. Chen and R. El-Ganainy, Nat. Electron. **2**, 323 (2019).
[32] P. Aleahmad, M. Khajavikhan, D. N. Christodoulides, and P. LiKamWa, Sci. Rep. **7**, 2129 (2017).
[33] H. Ramezani, T. Kottos, R. El-Ganainy, and D. N. Christodoulides, Phys. Rev. A **82**, 043803 (2010).
[34] R. El-Ganainy, L. Ge, M. Khajavikhan, and D. N. Christodoulides, Phys. Rev. A **92**, 033818 (2015).
[35] M. P. Hokmabadi, N. S. Nye, R. El-Ganainy, D. N. Christodoulides, and M. Khajavikhan, Science **363**, 623 (2019).
[36] Z. Gao, S. T. M. Fryslie, B. J. Thompson, P. S. Carney, and K. D. Choquette, Optica **4**, 323 (2017).
[37] Z. Gu, N. Zhang, Q. Lyu, M. Li, S. Xiao, and Q. Song, Laser Photonics Rev. **10**, 588 (2016).
[38] M. Liertzer, L. Ge, A. Cerjan, A. D. Stone, H. E. Tureci, and S. Rotter, Phys. Rev. Lett. **108**, 173901 (2012).
[39] M. Brandstetter, M. Liertzer, C. Deutsch, P. Klang, J. Schöberl, H. E. Tureci, G. Strasser, K. Unterrainer, and S. Rotter, Nat. Commun. **5**, 4034 (2014).
[40] R. El-Ganainy, M. Khajavikhan, and L. Ge, Phys. Rev. A **90**, 013802 (2014).
[41] M. Sakhdari, N. M. Estakhri, H. Bagci, and P.-Y. Chen, Phys. Rev. Applied **10**, 024030 (2018).
[42] J. Wiersig, Phys. Rev. Lett. **112**, 203901 (2014).
[43] J. Wiersig, Phys. Rev. A **93**, 033809 (2016).
[44] W. Chen, Ş. K. Özdemir, G. Zhao, J. Wiersig, and L. Yang, Nature (London) **548**, 192 (2017).
[45] H. Hodaei, A. U. Hassan, S. Wittek, H. Garcia-Gracia, R. El-Ganainy, D. N. Christodoulides, and M. Khajavikhan, Nature (London) **548**, 187 (2017).
[46] Q. Zhong, J. Ren, M. Khajavikhan, D. N. Christodoulides, Ş. K. Özdemir, and R. El-Ganainy, Phys. Rev. Lett. **122**, 153902 (2019).
[47] M. Sakhdari, M. Farhat, and P.-Y. Chen, New J. Phys. **19**, 065002 (2017).
[48] R. El-Ganainy, J. I. Dadap, and R. M. Osgood, Opt. Lett. **40**, 5086 (2015).
[49] Q. Zhong, A. Ahmed, J. I. Dadap, R. M. Osgood, and R. El-Ganainy, New J. Phys. **18**, 125006 (2016).
[50] R. El-Ganainy, K. G. Makris, M. Khajavikhan, Z. H. Musslimani, S. Rotter, and D. N. Christodoulides, Nat. Phys. **14**, 11 (2018).
[51] L. Feng, R. El-Ganainy, and L. Ge, Nat. Photonics **11**, 752 (2017).
[52] J. Doppler, A. A. Mailybaev, J. Böhm, U. Kuhl, A. Girschik, F. Libisch, T. J. Milburn, P. Rabl, N. Moiseyev, and S. Rotter, Nature (London) **537**, 76 (2016).
[53] H. Xu, D. Mason, L. Jiang, and J. G. E. Harris, Nature (London) **537**, 80 (2016).
[54] Q. Zhong, M. Khajavikhan, D. N. Christodoulides, and R. El-Ganainy, Nat. Commun. **9**, 4808 (2018).
[55] H. Gan, Ph. D. Thesis, Stanford University, 006.

[56] D. Gilles and G. Eva-Maria, J. Phys. A **45**, 025303 (2012).
[57] M. H. Teimourpour, R. El-Ganainy, A. Eisfeld, A. Szameit, and D. N. Christodoulides, Phys. Rev. A **90**, 053817 (2014).
[58] M. H. Teimourpour, Q. Zhong, M. Khajavikhan, and R. El-Ganainy, in *Parity-Time Symmetry and Its Applications*, edited by D. Christodoulides and J. Yang (Springer Singapore, Singapore, 2018), pp. 261–275.
[59] See Supplemental Material at http://link.aps.org/supplemental/10.1103/PhysRevLett.123.193901 for effective *PT* symmetric Hamiltonian for three coupled oscillators, rf reader design and wireless measurement setups, schematics and experimental setups, magnitude of the reflection coefficient versus frequency, and measurement precision, which includes Refs. [23,60–62].
[60] L. Ge, Phys. Rev. A **95**, 023812 (2017).
[61] S. Malzard, C. Poli, and H. Schomerus, Phys. Rev. Lett. **115**, 200402 (2015).
[62] Keysight E5061B ENA Vector Network Analyzer, https://literature.cdn.keysight.com/litweb/pdf/5990-4392EN.pdf.